Study of vibration control using laboratory test rig of wind turbine tower-nacelle system with MR damper based tuned vibration absorber

P. MARTYNOWICZ*

AGH University of Science and Technology, Department of Process Control, 30 Mickiewicza Ave., 30-059 Krakow, Poland

Abstract. Wind turbine tower dynamic stress is related to the fatigue wear and reliability of the whole wind turbine structure. This paper deals with the problem of tower vibration control using a specially designed and built laboratory model. The considered wind turbine tower-nacelle model consists of a vertically arranged stiff rod (representing the tower), and a system of steel plates (representing nacelle and turbine assemblies) fixed at its top. The horizontally aligned tuned vibration absorber (TVA) with magnetorheological (MR) damper is located also at the top of the rod (in nacelle system). Force excitation sources applied horizontally to the tower itself and to the nacelle were both considered. The MR damper real-time control algorithms, including ground hook control and its modification, sliding mode control, linear and nonlinear (cubic and square root) damping, and adaptive solutions are compared to the open-loop case with various constant MR damper input current values and system without MR TVA (i.e., MR TVA in "locked" state). Comprehensive experimental analyses and their results are presented.

Key words: wind turbine vibration, tower-nacelle laboratory model, tuned vibration absorber, MR damper, tower vibration control.

1. Introduction

One of the emerging renewable energy sectors nowadays is wind turbines industry. Wind turbines are ecological solutions; however, their implementation cost is significant. Structural vibration and its consequences imply appropriately high investment into construction process and it is one of the greatest contributors to the total amount of wind farm implementation costs. The wind load (and also sea waves load for the offshore structures) which varies in time as well as rotation of turbine elements are the major contributors to the structural vibration of tower and blades. Cyclic stress that the tower is subjected to may lead to the decrease in reliable operation time due to structure fatigue wear [1] or even failure accident. Tower vibration arises due to various excitation sources as variable wind conditions, including wind shear, Karman vortices, blade passing effect, differences in inflow conditions for each of the blades, rotating elements unbalance, generator operation, sea waves, ice, etc [2]. This vibration is generally lightly damped, especially considering low aeroelastic damping for the first tower lateral mode [3–6]. The lateral modes are excited due to Karman vortices, generator operation, sea waves' variable load and rotating machinery unbalance, rather than due to direct wind load variation and blade passing effect, as for longitudinal modes. In the project presented, only the tower vibration is analyzed.

The solutions utilized to reduce wind turbines towers' vibration include collective blade pitch control, generator electromagnetic torque control [7–9], and passive, semi-active, or active tuned vibration absorbers (TVAs) [10–13]. TVAs are widely spread structural vibration reduction solutions for slender structures. In the standard (passive) approach, TVA consists of the additional moving mass, spring and viscous damper, which parameters are tuned to the selected (most often first) mode of vibration [10, 14]. Passive TVAs work well at the load conditions characterized with a single frequency to which they are tuned, but cannot adapt to wide excitation spectrum [15], thus more advanced TVAs are considered to change or tune TVA operating frequency. Among them, magnetorheological (MR) TVAs are placed [15], as using MR damper (instead of viscous damper) guarantees a wide range of resistance force, fast response times, low sensitivity to temperature change and fluid contamination, high operational robustness, and minor energy requirements as compared with active systems [16–18]. As simulations and experiments show, implementation of MR damper in TVA system may lead to further vibration reduction in relation with passive TVA (subject of author's separate publications).

Within the scope of current project, tower-nacelle simulation and laboratory models (Figs. 1 and 2) were specially developed and built, in which all turbine components (nacelle, blades, hub, shaft, generator and possibly gearbox) are represented by nacelle concentrated mass and mass moments of inertia. The laboratory test rig of wind turbine tower-nacelle system offers the possibility of modeling tower vibration under various aerodynamic, hydrodynamic, mechanical unbalance, changeable electromagnetic load, and other excitation sources (listed above), since horizontal concentrated force (designated by $F_s(t)$) generated by dedicated shaker may be applied to the nacelle, or to the tower itself at different heights if necessary. Several initial modes of vibration may be analyzed. The rig may also be laid down on the horizontally excited platform to model vibration of buoy-floating wind turbine structures, or vibration due to seismic excitation.

Various approaches to the problem of wind turbine tower vibration control with MR TVA are presented. With the use of MR damper, standard TVA linear (viscous) damping algorithm may

*e-mail: pmartyn@agh.edu.pl

be realized as well as more advanced controllers. Throughout them, ground hook control and its modification, sliding mode control, linear and nonlinear damping, and adaptive control algorithms are implemented, in comparison to open-loop solutions with several MR damper input current values and system without TVA (i.e. TVA in "locked" state). Only the first bending mode of vibration is analyzed here. Two independent, horizontal, concentrated force excitation sources are considered: the first one applied to the nacelle, the second one, to the tower midpoint.

The paper is organized as follows. In the forthcoming section, wind turbine tower-nacelle model is introduced. Then, laboratory test rig with measurement and control system is presented. Vibration control algorithms are followed by the experimental results. The paper ends with several conclusions.

2. Wind turbine tower-nacelle model

The model to be analyzed (Fig. 1) consists of stiff rod (*Tower*) arranged vertically, representing wind-turbine tower, and a stiff body connected rigidly to the top of the rod, representing both nacelle and turbine assemblies (*Nacelle*). The bottom end of the rod is fixed to the ground via additional foundation. As the first tower bending mode has dominant modal mass participation (ca. fivefold greater than the next mode), vibration reduction system that comprises spring and MR damper (built in parallel) with an additional stiff body (*Absorber*), operating all together as TVA, is located at the top of the tower (at *Nacelle*). The horizontal disturbance load, provided in the laboratory conditions by the dedicated modal shaker, may either be concentrated at the nacelle, or applied to the arbitrary tower section; both locations enable forcing tower bending modes of vibration. The MR TVA direction of operation is the same as the direction of applied excitation (assuming small bending angles).

Based on all the assumptions, constraints and thorough analyses results that are covered in [19–21], Ti Gr. 5 rod was selected to model wind turbine tower, while Lord Co. RD 1097-1 [17] was utilized as TVA MR damper. The parameters of TVA were tuned for the first bending mode of vibration [10, 14]. The absorber mass m_2 after several system reconfigurations was selected to be ca. 15% of the modal mass of the first bending mode of tower-nacelle model m_1 (i.e. mass ratio was $\mu = m_2/m_1 = 0.152$).

3. Laboratory test rig

A laboratory test rig of wind turbine tower-nacelle system (Fig. 2) was built according to the details specified above. It consists of a vertically oriented titanium (Ti Gr.5) rod *1* (representing wind-turbine tower), and a system of steel plates *2* (representing nacelle and turbine assemblies) fixed to the top of the rod *1*, with MR TVA embedded. The titanium rod is rigidly mounted to adequately large and stiff steel foundation frame *3*. MR TVA *4* is an additional mass moving horizontally along linear bearing guides, connected with the system representing nacelle via spring and Lord RD 1097-1 MR damper [17] in parallel. RD 1097-1 damper (whose force depends on

the current fed to its coil) is an actuator of such a vibration reduction system. MR TVA operates along the same direction as vibration excitation applied to the system. Force generated by vibration excitation system, i.e., the Modal Shop lightweight electrodynamic force exciter *5* of 2060E series (TMS 2060E) [22] with drive train assembly *6* of changeable leverage (enabling changeable force, displacement and velocity ranges) may be applied either to the rod *1* (modelling the tower, as in the picture) or to the set of steel plates *2* modelling nacelle/turbine. Excitation signal is generated by LDS Dactron *7* and amplified by the Modal Shop 2100E21-400 unit *8*. Such a laboratory test rig gives the possibility to model wind turbine tower vibration under several excitation sources [19–21].
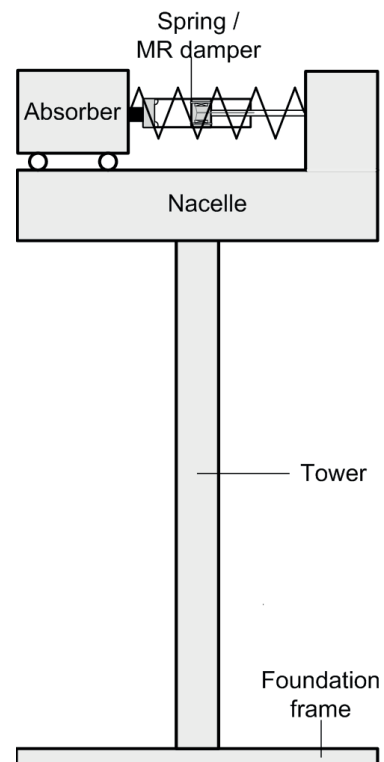

Fig. 1. Sketch of the tower-nacelle model with MR TVA

Measurement and control system (Fig. 3) consists of laser displacement transducer / laser vibrometer with its controller *9* for rod *1* tip (and system *2*) horizontal displacement (x_1) / velocity ($\dot{x}_1$) measurement, laser displacement transducer *10* for rod *1* midpoint horizontal displacement measurement (x_0) (at half of rod length), LVDT transducer *11* for system *2* – TVA *4* relative displacement (x_1-x_2) measurement, tensometric stress transducers *12*, MR damper force (P_{MR}), shaker force, and acceleration transducers (not apparent in Fig. 2), as well as transducers supply/amplifying/conditioning system including MR damper current controller *13*, and measuring-control PC *14* with MATLAB/Simulink/RT-CON applications (signals designations listed in brackets). The operation of MR damper current controller is apparent in Fig. 7 – see time pattern of measured control voltage u_{MR} (*vs. measured* current i_{MR}) as an

Study of vibration control using laboratory test rig of wind turbine tower-nacelle system with MR damper based tuned vibration absorber
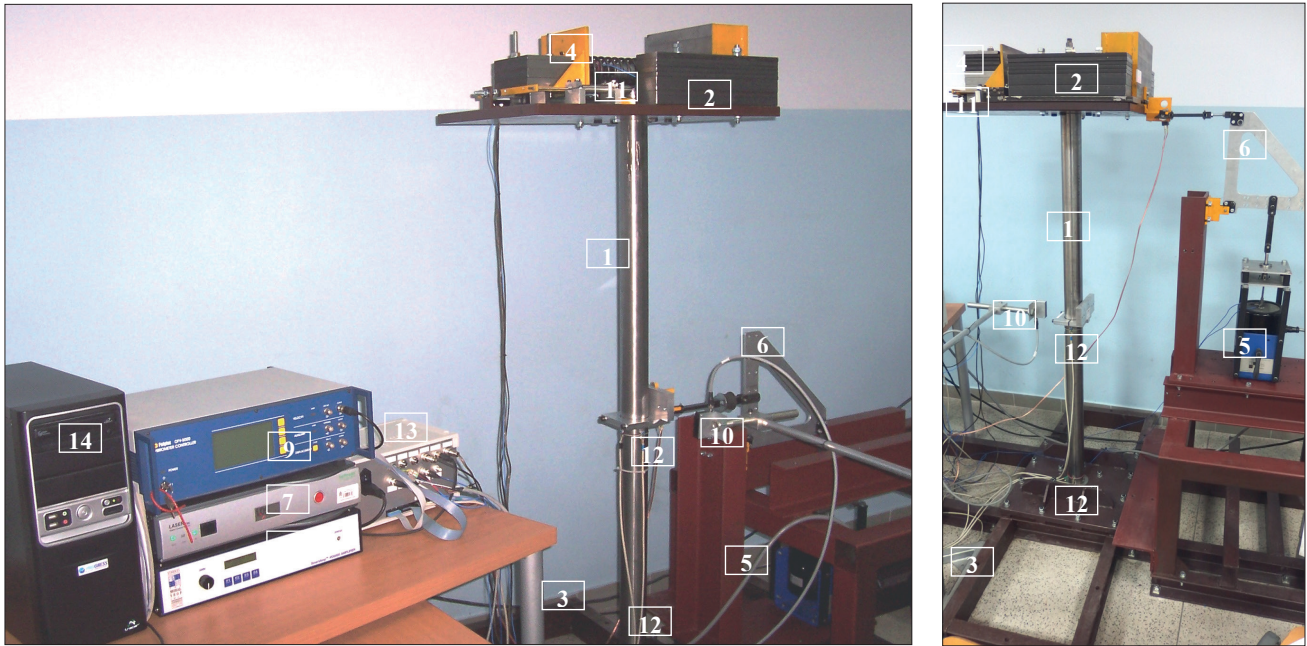

Fig. 2. Laboratory test rig: excitation applied to the tower midpoint (left) or to the nacelle (right)
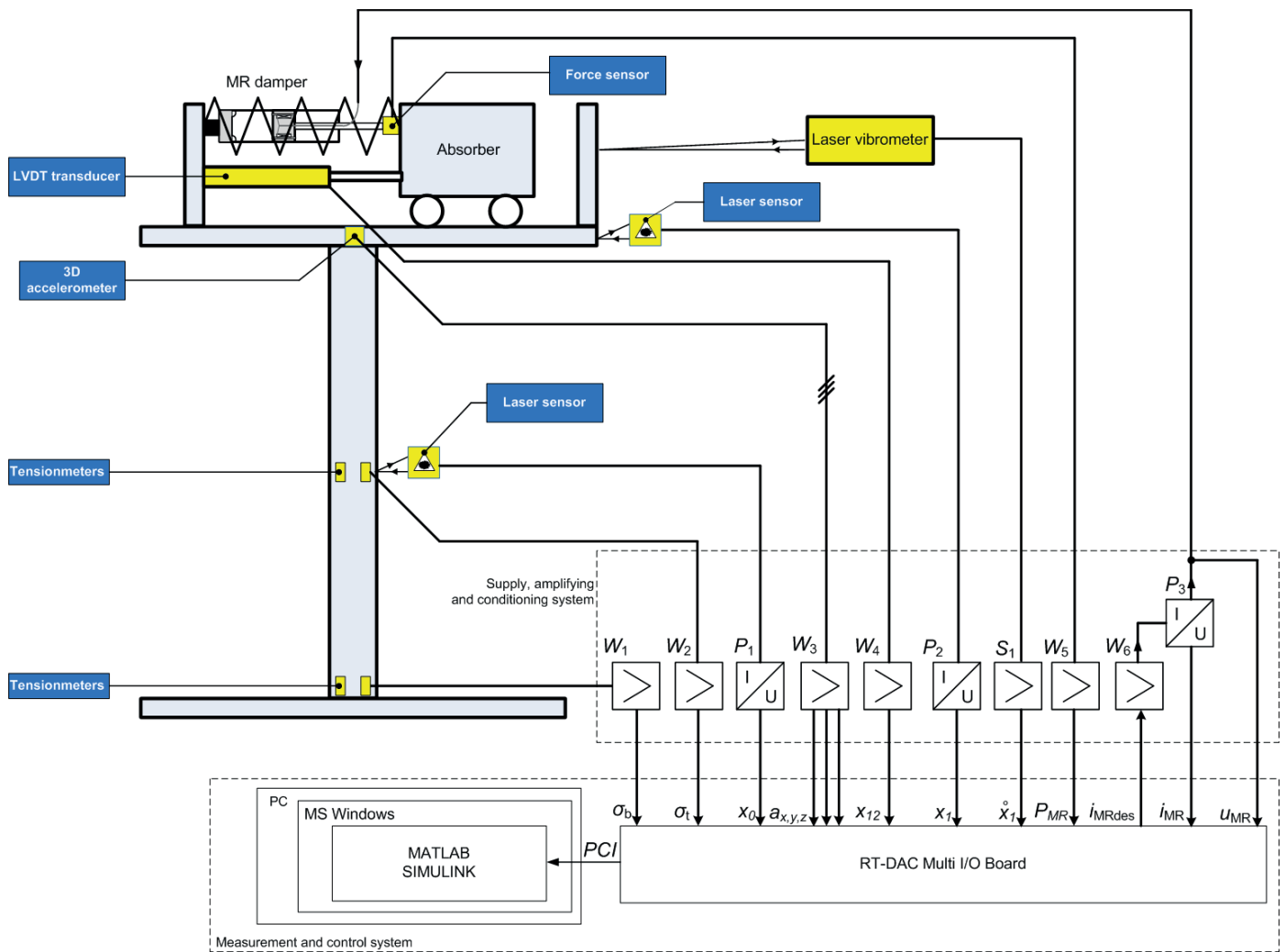

Fig. 3. Measurement and control system diagram

output of analogue PID controller embedded in *13* to force required current pattern. Data acquisition and control system diagram is presented in Fig. 3.

Selected test rig parameters are presented in Table 1, while the entire identification problem is covered in [23]. FFTs exhibiting averaged 1st (f_1=3.45 Hz) and 2nd (f_2=30.52 Hz) bending frequencies of the laboratory and simulation models [23–26], obtained from the experimental $|x_0(f)|$ and simulation $|x_{0M}(f)|$ rod midpoint horizontal displacement series, are presented in the Fig. 4.

Table 1
Parameters of tower-nacelle laboratory test rig.

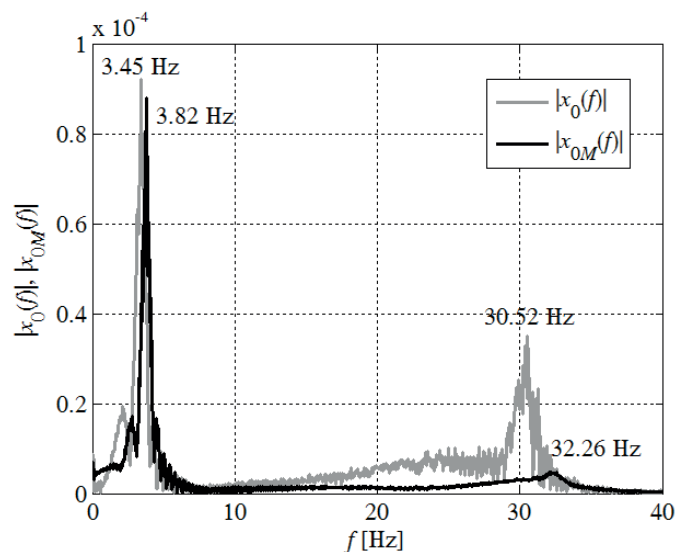| Parameter	Value
Length of the rod (tower) [10^{-3} m]	1507
Diameter of the rod [10^{-3} m]	70.50
Mass of the rod [kg]	26.06
Mass of the system located at the top of the rod (nacelle) w/o TVA [kg]	163.40
TVA absorber mass [kg]	25.78
TVA optimal stiffness coefficient [10^3 N/m]	13.41
TVA optimal damping coefficient [Ns/m]	227.2

Fig. 4. FFTs calculated from experimental ($|x_0(f)|$) and simulation ($|x_{0M}(f)|$) rod midpoint displacement patterns (presented in a separate publication on test rig identification [23])

4. Vibration control

Considering nonzero MR damper response time and value of the 2nd bending mode frequency (separate publication on test rig identification), the main purpose of vibration reduction system and TVA implementation was to reduce amplitudes of x_0 (rod midpoint) and x_1 (rod tip or nacelle) horizontal displacements corresponding to 1st tower-nacelle bending mode, thus TVA location was selected to be at the nacelle [19, 21, 24, 26]. In this paper, selected approaches to the problem of wind turbine tower-nacelle system vibration control with MR TVA are pre-

sented using specially developed and built laboratory test rig, on the basis of previous thorough simulations and preliminary experiments including 1st and 2nd bending mode of vibration analyses that are presented in [24, 26]. Since it was observed that 2nd bending mode of vibration reduction possibilities for the system with MR TVA are negligible, only the 1st mode of vibration is analyzed here. Using MR damper, standard TVA linear damping algorithm [10] implementation results (designated by *C*) are compared with results of ground hook (*GND*) and modified ground hook (*Mod.GND*), sliding mode (*SMC*), nonlinear damping including cubic (*C3*) and square root damping (*SQRT*), adaptive (*ADPT*) and open-loop solutions with constant MR damper input current of 0.0A, 0.1A, and 0.2A, and system with TVA "locked" by one-sided bolt and MR damper input current of 1.0 A.

Two independent force excitation sources are considered. The force (designated by F_s) applied to the rod *1* itself at half of its height through the drive train assembly *6* (see Fig. 2) represents direct or indirect external (aerodynamic, sea waves, ice, etc.) tower loads that may be reduced to the resultant concentrated force applied at half of tower height. The load applied horizontally to the system *2* modelling the nacelle (P_s) represents mainly wind thrust on the tower top / nacelle through the rotor.

The aim of MR damper implementation was to improve TVA vibration reduction capabilities in relation with standard (passive) solution with linear damper of constant damping coefficient, especially to decrease displacement amplitudes corresponding to the two local maxima apparent in the frequency response of typical structure with TVA. Real-time control strategies implemented to determine MR damper input current are listed below. The author's idea of ground-hook algorithm modification is discussed elaborately at the end of the section, as other control strategies are only mentioned here following their introduction in [26] and partially in [24].

4.1. Linear damping (C). In this approach, MR damper is used to emulate linear (viscous) damper of optimally tuned TVA damping coefficient c_2 with k_2 being optimally tuned stiffness coefficient [10, 14, 24, 26]. As previous results proved, the laboratory model is more damped than simulation one (and that compromised MR damper control possibilities) due to e.g. MR damper pre-yield component that is most significant at low velocities, absorber linear bearing guides friction, interfacial slip in joints, linear damping with reduced c_2 value ($0.6c_2$) was also tested (designations *1C* or *0.6 C*).

Internal feedback P-controller loop (alternatively to PI-controller [27] with settings as in [24, 26]) with MR damper real-time force measurement is implemented in such a force follow-up algorithm [24, 26, 27]. P-controller proportional gain is 0.04, saturation limits are (0, 1) A, and a measurement signal scaling factor (*alpha*) is equal to 0.75.

Apart from P (PI) loop with MR damper force measurement (Fig. 3) operating as MR damper force follow-up algorithm, for selected (most adequate) algorithm versions control current may also be determined with the use of MR damper hyperbolic tangent inverse model Simulink implementation, which inputs are desired force, relative displacement and velocity, and output is

www.czasopisma.pan.pl   PAN   www.journals.pan.pl

Study of vibration control using laboratory test rig of wind turbine tower-nacelle system with MR damper based tuned vibration absorber

control current for the damper [26]. Analysis concerning the use of inverse model with hysteresis or without was conducted, as hysteresis introduced ambiguity. If MR damper inverse model was used instead of P (PI) control loop, designation in graphs/table *INV* is present, while for P (PI) follow-up algorithm designation *P (PI1)* is apparent.

4.2. Nonlinear damping (C3 and SQRT). This solution is MR damper based implementation of nonlinear damping [26–28] in (MR) TVA system. Two approaches considered here are:

- cubic damping with MR damper desired force calculated as: $P_{MR}^{desired} = K_3 c_2 (\dot{x}_1 - \dot{x}_2)^3$, with several K_3 values: K_3=50, K_3=150, K_3=250, and K_3=500 selected on the basis of simulation and experimental analyses (designations: *C3 50*, *C3 150*, *C3 250*, and *C3 500*, respectively),
- square-root damping with MR damper desired force calculated as: $P_{MR}^{desired} = K_{1/2} c_2 \, \mathrm{sgn}(\dot{x}_1 - \dot{x}_2) \sqrt{|\dot{x}_1 - \dot{x}_2|}$, with $K_{1/2}$=0.05, $K_{1/2}$=0.15, $K_{1/2}$=0.25, and $K_{1/2}$=0.45 selected on the basis of previous analyses (designations in graphs: *SQRT 0.05*, *SQRT 0.15*, *SQRT 0.25* and *SQRT 0.45*, respectively).

Both nonlinear damping approaches comprise force follow-up control algorithms mentioned in *Linear damping (C)* section, and selected versions use MR damper inverse model.

4.3. Adaptive control (ADAPT). An adaptive control implemented here is based on utilizing MR damper to emulate controllable stiffness and controllable viscous damping in such a way that TVA stiffness $k_2^{adapt} = k_2^{desired}$ and damping $c_2^{adapt} = c_2^{desired}$ coefficients are tuned to the excitation frequency rather than to tower-nacelle system 1st bending frequency (as k_2 and c_2 in *Linear damping (C)* section), using dependencies [10, 14, 26]. Additionally, solutions with reduced damping coefficient, i.e. $c_2^{adapt} = 0.6 c_2^{desired}$, and $c_2^{adapt} = 0$ were analyzed (designation: *ADAPT 1C*, *ADAPT 0.6C* or *ADAPT 0C*) – damping reduction at the frequency to which TVA is tuned should lead to vibration mitigation at this frequency (equal to excitation frequency; applicable for single-frequency excitation spectrum). Thus, real-time determination of excitation frequency is followed by real-time calculation of TVA required stiffness: $P_{stiff} = k_2^{adapt}(x_1 - x_2)$, and damping: $P_{damp} = c_2^{adapt}(\dot{x}_1 - \dot{x}_2)$ forces, leading to MR damper desired force formula:

$$P_{MR}^{desired} = \left(k_2^{adapt} - k_2\right)(x_1 - x_2) + c_2^{adapt}(\dot{x}_1 - \dot{x}_2), \quad (1)$$

where k_2 is spring stiffness determined on the basis of standard TVA tuning to tower-nacelle system 1st bending frequency. As MR damper cannot deliver energy to the system, force (8) cannot be exactly mapped either. Thus, a dedicated force follow-up PI-based control algorithm was specially developed [26] with (0, 1) A saturation range (designation in graphs: *PI2*). PI controller settings were as in [26]. Alternatively inverse model was used (*INV*).

4.4. Sliding mode control (SMC). Sliding mode (nonlinear control strategy) is widely used due to its robustness and ability to decouple high-dimension systems into a set of independent lower-dimension subsystems [29, 30]. Only the dynamics of

the 1st bending mode modal mass with TVA was considered, with sliding surface: $s = x_1 + \dot{x}_1$. MR damper input current i_{MR} control law may be expressed by [29]:

$$i_{MR} = \begin{cases} i_{MR}^{max}, & \mathrm{sign}\left[s(\dot{x}_1 - \dot{x}_2)\right] = 1 \\ 0, & \mathrm{sign}\left[s(\dot{x}_1 - \dot{x}_2)\right] \neq 1 \end{cases}, \quad (2)$$

where $i_{MR}^{max} = 0.25, i_{MR}^{max} = 0.5$, or $i_{MR}^{max} = 1.0$ A values were selected (designations: *SMC 0.25*, *SMC 0.5*, *SMC 1.0*) [26].

4.5. Ground-Hook control (GND). The implementation of this simple strategy for slender structures provides vibration reduction (with relation to the ground) that is most efficient at the point of (MR) TVA / *GND* application. The MR damper input current i_{MR} control algorithm (displacement ground-hook version) is represented by the formula:

$$i_{MR} = \begin{cases} i_{MR}^{max}, & x_1(\dot{x}_1 - \dot{x}_2) \geq 0 \\ 0, & x_1(\dot{x}_1 - \dot{x}_2) < 0 \end{cases}. \quad (3)$$

On the basis of previous analyses $i_{MR}^{max} = 0.25$, or $i_{MR}^{max} = 0.5$ were selected (designations: *GND 0.25*, *GND 0.5*) [26].

4.6. Modified Ground-Hook control (Mod.GND). The ground-hook modification idea presented here is based on standard displacement version of ground hook algorithm as mentioned above. In formula (3), MR damper input current is intended to be maximal when signs of structure absolute displacement x_1 and structure–TVA relative velocity $\dot{x}_1 - \dot{x}_2$ are the same. It was observed, however, that MR damper force should be maximal when signs of structure absolute displacement x_1 and MR damper force P_{MR} are the same (rather than signs of x_1 and $\dot{x}_1 - \dot{x}_2$). During sine excitation test, for some part of the period MR damper behaves as an "active" device (observing force-velocity plot in Fig. 5). Although velocity $\dot{x}_1 - \dot{x}_2$ sign is opposite to displacement x_1 sign, MR damper force sign P_{MR} is the same as x_1 sign, thus it may be used for vibration mitigation by maximizing MR damper force in that time (Figs. 6 and 7). As can be seen in Figs. 7 and 8, *Mod.GND* control is much more precise as it concerns time instants at which damper force should be increased (resulting in $A(x_1)$ reduction), as compared to *GND* control. This situation appears for a short part of sine period and results from MR damper hysteresis phenomenon. This is not the case in TVA system with viscous damper.

The idea underlying the modified ground-hook algorithm implemented on MR damper takes a simple form:

$$i_{MR} = \begin{cases} i_{MR}^{max}, & x_1 P_{MR} \geq 0 \\ 0, & x_1 P_{MR} < 0 \end{cases} \quad (4)$$

with emphasis put on bias cancellation algorithm for both x_1 and P_{MR} signals; $i_{MR}^{max} = 0.25$, or $i_{MR}^{max} = 0.5$ (designations: *Mod. GND 0.25*, *Mod.GND 0.5*) were selected on the basis of previous simulation and experimental analyses [26].
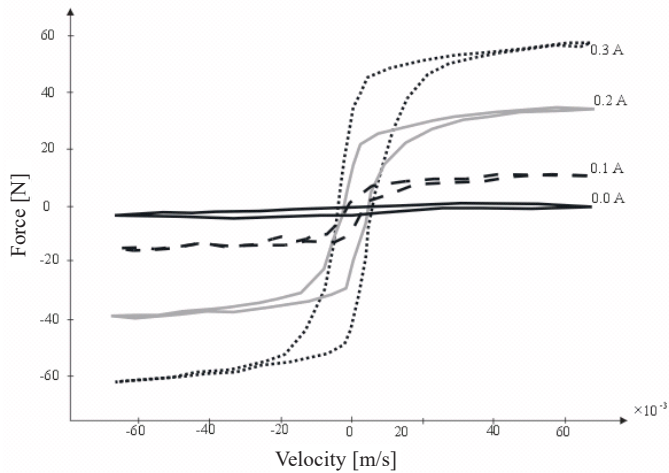
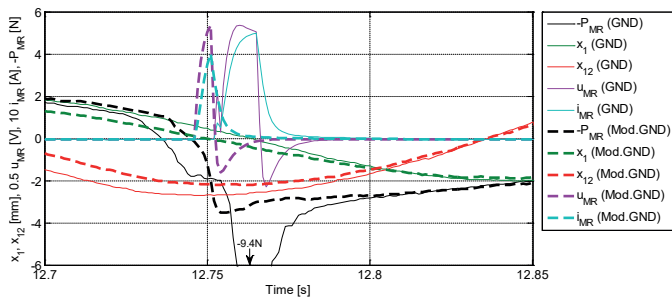Fig. 5. RD 1097-1 exemplary force-velocity plots, sine excitation

Fig. 6. Modified ground hook underlying idea, $f = 2.95$ Hz, GND0.5 vs. Mod.GND0.5 (see Fig. 15)
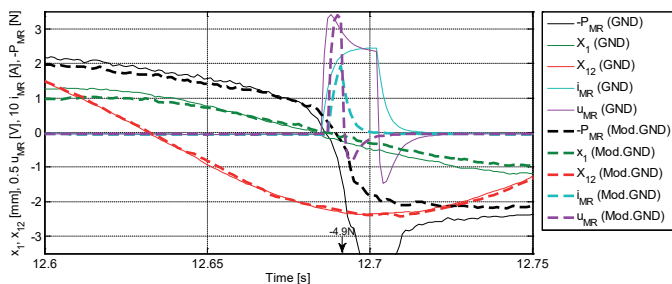

Fig. 7. Modified ground hook underlying idea, $f = 3.45$ Hz, GND0.25 vs. Mod.GND0.25 (see Fig. 15)

5. Laboratory tests

Initial laboratory tests as well as system identification and dynamic similarity analysis procedures and results are presented as separate publications [23–26].

The control algorithms presented in previous section were implemented and tested on the laboratory test rig in comparison with open-loop (passive) system with constant MR damper input currents: 0.0 A, 0.1 A, and 0.2 A, standard *LQG* approach [31] and a system without TVA in operation (TVA "locked"). Whether linear or nonlinear damping, or adaptive solution was used (demanding determination of control current on the basis of calculated desired force), desired force was

augmented by minus kinetic friction force produced, during operation of absorber linear bearing guides, that was estimated to be of the order of 1 N using MR damper force sensor (Fig. 3) with the damper "locked" by 1.0 A input current for constant velocity draw/pull test. Compensation of friction force was indicated in frequency characteristics by designation *Fr*. Two excitation configurations were investigated during the tests, as in Fig. 2.

The first test aimed to determine amplitude of x_0 and x_1 output frequency response functions (A(x_0), A(x_1) respectively), so series of experiments were conducted at selected discrete sine excitation frequency points within the range of (2.55, 5.05) Hz with a step of 0.1 Hz, comprising 1st bending frequency region of the system without TVA. The system was excited by a force of amplitude $A(F_s(t)) = 150$ N applied to the rod (tower) midpoint.

Figs. 8–13 present A(x_0) displacement amplitude output frequency response functions for open-loop and feedback systems with control current and control algorithms details included in figures' legends. Analogously, Figs. 14–19 present A(x_1) output frequency response functions. Fig. 20 presents $A(x_0)$ and $A(x_1)$ output frequency response functions for the system without MR TVA (TVA "locked"). All of these characteristics are presented in combination with output frequency response functions of control system that was recognized as a best MR TVA option (concerning vibration frequency responses) on the experimental laboratory ground, i.e. *Mod. GND* algorithm with maximum control current of 0.5 A. The maximum amplitudes obtained for *Mod.GND* are ca. 10 times smaller than for the system without TVA regarding the whole frequency range.
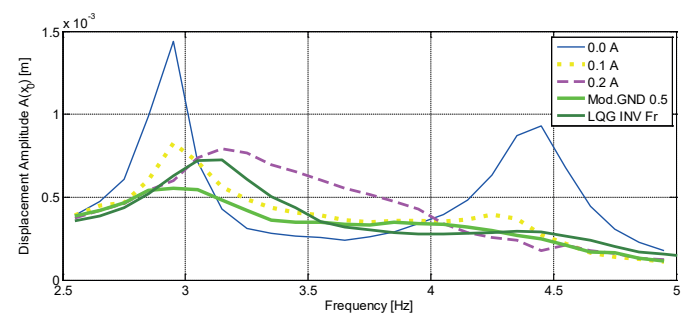

Fig. 8. Tower midpoint displacement amplitude $A(x_0)$ output frequency response functions for the system with MR TVA, $A(F_s(t))=150$ N (details in the text and in the legend)
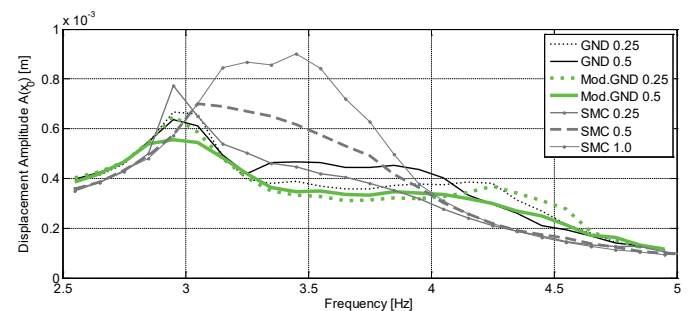

Fig. 9. Tower midpoint displacement amplitude $A(x_0)$ output frequency response functions for the system with MR TVA, $A(F_s(t))=150$ N
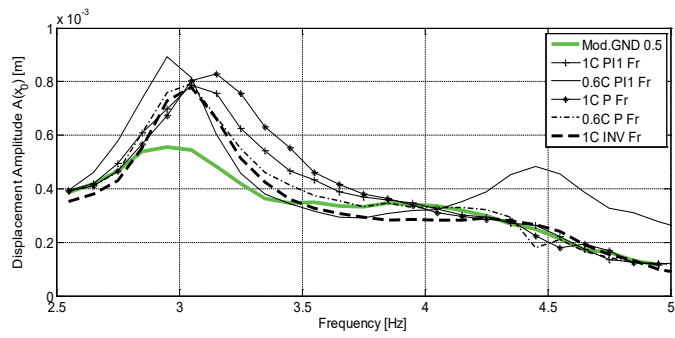
Study of vibration control using laboratory test rig of wind turbine tower-nacelle system with MR damper based tuned vibration absorber

Fig. 10. Tower midpoint displacement amplitude $A(x_0)$ output frequency response functions for the system with MR TVA, $A(F_s(t))=150$ N

Fig. 11. Tower midpoint displacement amplitude $A(x_0)$ output frequency response functions for the system with MR TVA, $A(F_s(t))=150$ N
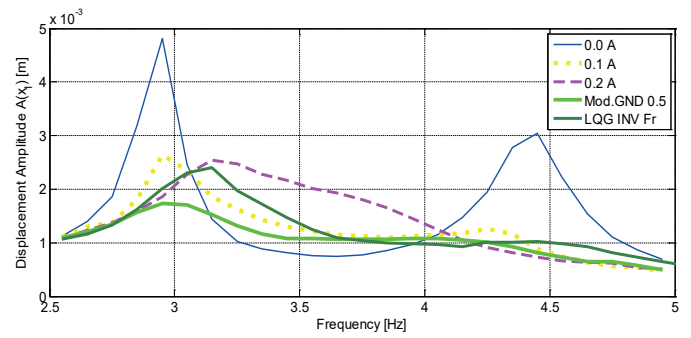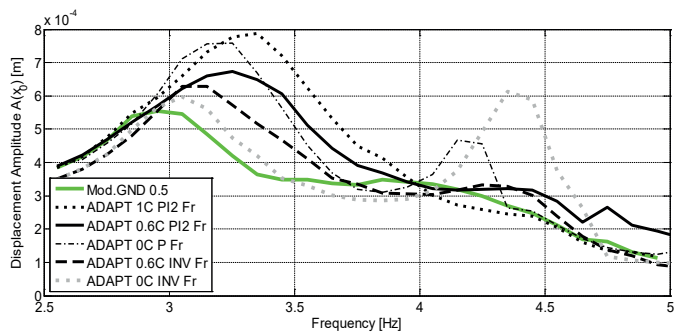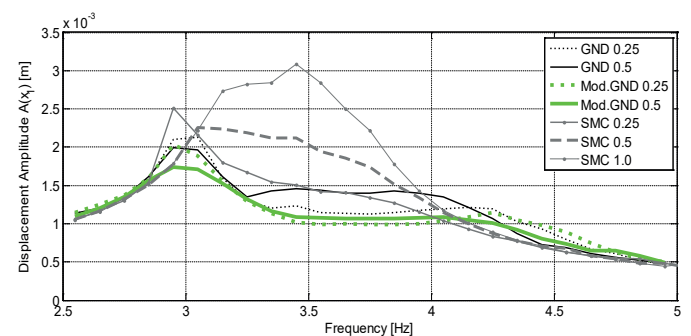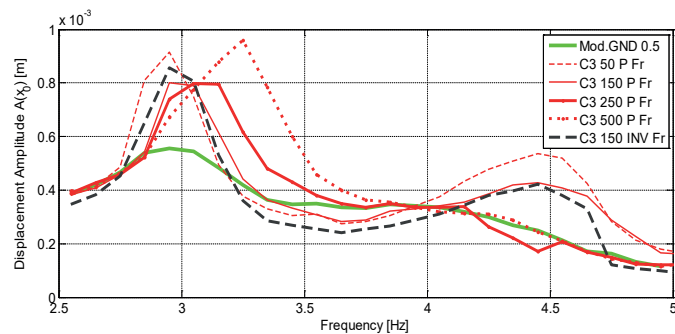

Fig. 12. Tower midpoint displacement amplitude $A(x_0)$ output frequency response functions for the system with MR TVA, $A(F_s(t))=150$ N
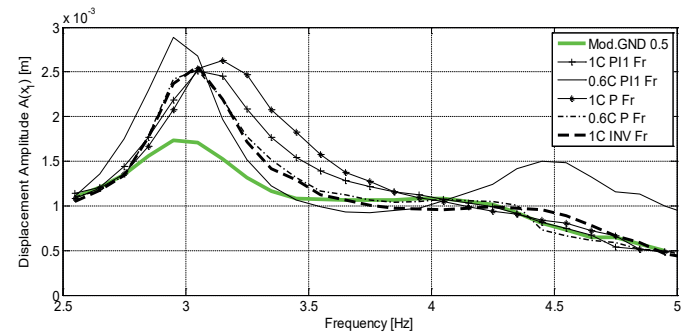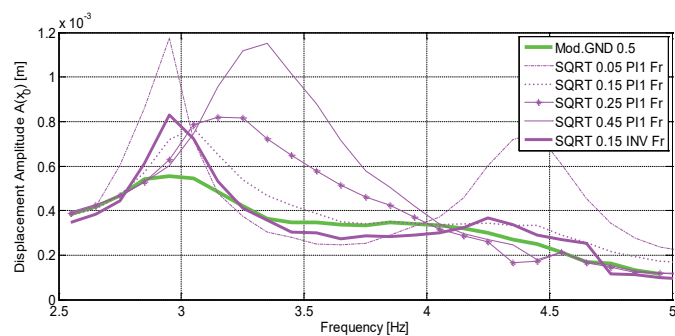

Fig. 13. Tower midpoint displacement amplitude $A(x_0)$ output frequency response functions for the system with MR TVA, $A(F_s(t))=150$ N

Fig. 14. Tower tip displacement amplitude $A(x_1)$ output frequency response functions for the system with MR TVA, $A(F_s(t)) = 150$ N

Fig. 15. Tower tip displacement amplitude $A(x_1)$ output frequency response functions for the system with MR TVA, $A(F_s(t))=150$ N

Fig. 16. Tower tip displacement amplitude $A(x_1)$ output frequency response functions for the system with MR TVA, $A(F_s(t))=150$
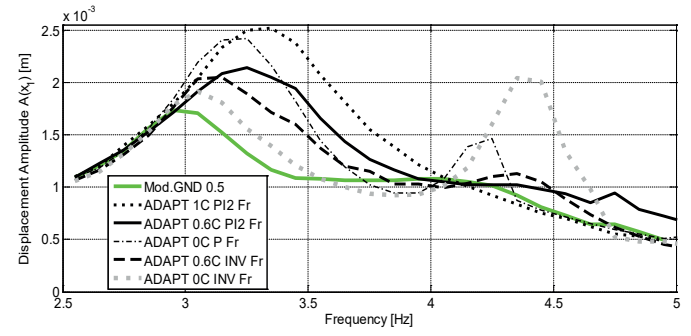

Fig. 17. Tower tip displacement amplitude $A(x_1)$ output frequency response functions for the system with MR TVA, $A(F_s(t))=150$ N
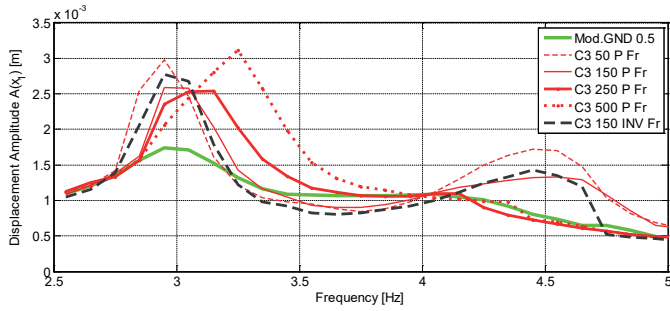
Fig. 18. Tower tip displacement amplitude $A(x_1)$ output frequency response functions for the system with MR TVA, $A(F_s(t))=150$ N
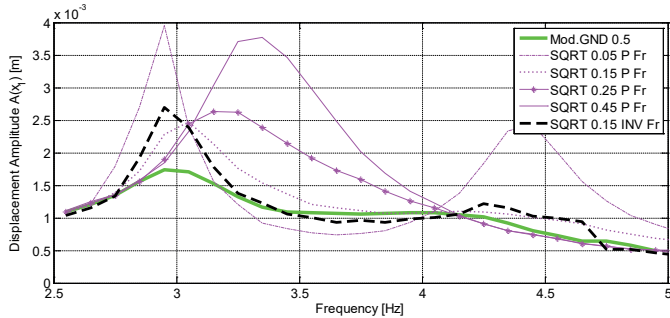

Fig. 19. Tower tip displacement amplitude $A(x_1)$ output frequency response functions for the system with MR TVA, $A(F_s(t))=150$ N
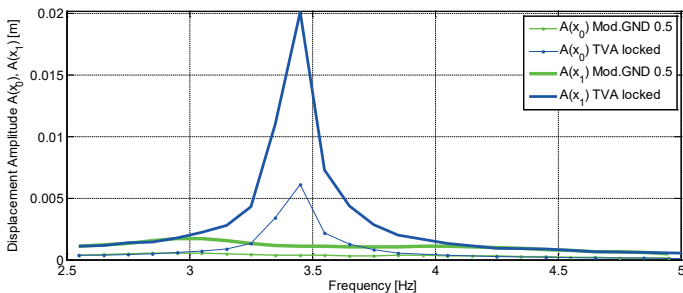

Fig. 20. Tower midpoint displacement amplitude $A(x_0)$ and tower tip displacement amplitude $A(x_1)$ output frequency response functions for the system with and without MR TVA, $A(F_s(t))=150$ N
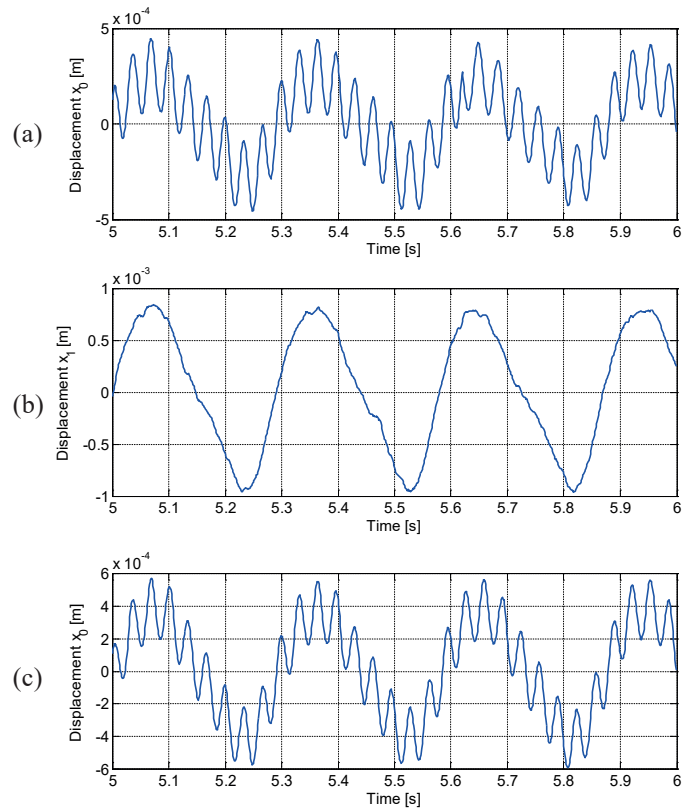
The next test was polyperiodic excitation applied both to the rod midpoint and to the system modelling the nacelle. The polyperiodic signal was a sum of the 1st bending frequency $f_1 = 3.45$ Hz and its second and third harmonics, and the 2nd bending frequency of $f_2 = 30.52$ Hz. Amplitude of each of the monoperiodic wave was 150N (regarding excitation at the rod/tower midpoint F_s) or 48.75N (regarding excitation at the nacelle P_s). As rod stiffness is inversely proportional to the length to the power of three, excitation applied to the system modelling the nacelle (although ca. three times smaller in amplitude) was more efficient in exciting the structure. Thus, it was selected for quantitative analysis (Table 2), while time responses obtained for rod midpoint excitation were used for graphical illustration (Fig. 21) only. The greater displacement amplitudes, the influence of friction forces of absorber linear bearing guides, MR damper sealing, MR damper pre-yield friction component etc. is less meaningful and so the inherent damping is smaller, i.e. more similar to the real-world case; thus, greater structure deflections

were preferred. However, it was observed that for polyperiodic excitation test that does incorporate high frequency content, the shaker and drive train system's ability to generate and transfer adequately high forces was slightly limited, which was not the case for the single frequency excitation test (presented above).

Quality indexes obtained for the selected systems and excitation P_s are gathered in Table 2 as amplitudes ($A(\cdot)$) of the steady state polyperiodic response. In each column of Table 2, index for the system with zero control current and for best (considering that index) of the remaining systems are all distinguished in bold. Fig. 21 presents time sections of polyperiodic responses for the system with MR

TVA at 0.0 A and 0.1 A control current (the latter recognized as the most favourable passive system, according to the frequency domain analysis), response for the system with TVA "locked", and the system with Mod.GND algorithm as well as excitation force F_s pattern. As can be observed, displacement x_0 exhibits both 1st and 2nd bending frequency for system with TVA, however for TVA "locked" 1st mode of vibration is dominant (2nd not visible) as its amplitudes are ca. 10 times greater than for the system with TVA in operation (TVA deals with 1st mode reduction only while 2nd mode is unaffected).

The system was then subjected to impulse excitation. The same selection of open-loop and feedback systems was made as for polyperiodic test. Considering the previously stated remark, response to the excitation applied to the system modelling the nacelle was used for quantitative analysis (Table 2), while excitation applied to the rod midpoint was used for graphical representation only. Results gathered in Table 2 are peak-peak displacements divided by two (($max(\cdot)-min(\cdot))/2$) and root-mean-square displacements ($RMS(\cdot)$). Fig. 22 presents time plots of

www.czasopisma.pan.pl   PAN   www.journals.pan.pl

Study of vibration control using laboratory test rig of wind turbine tower-nacelle system with MR damper based tuned vibration absorber

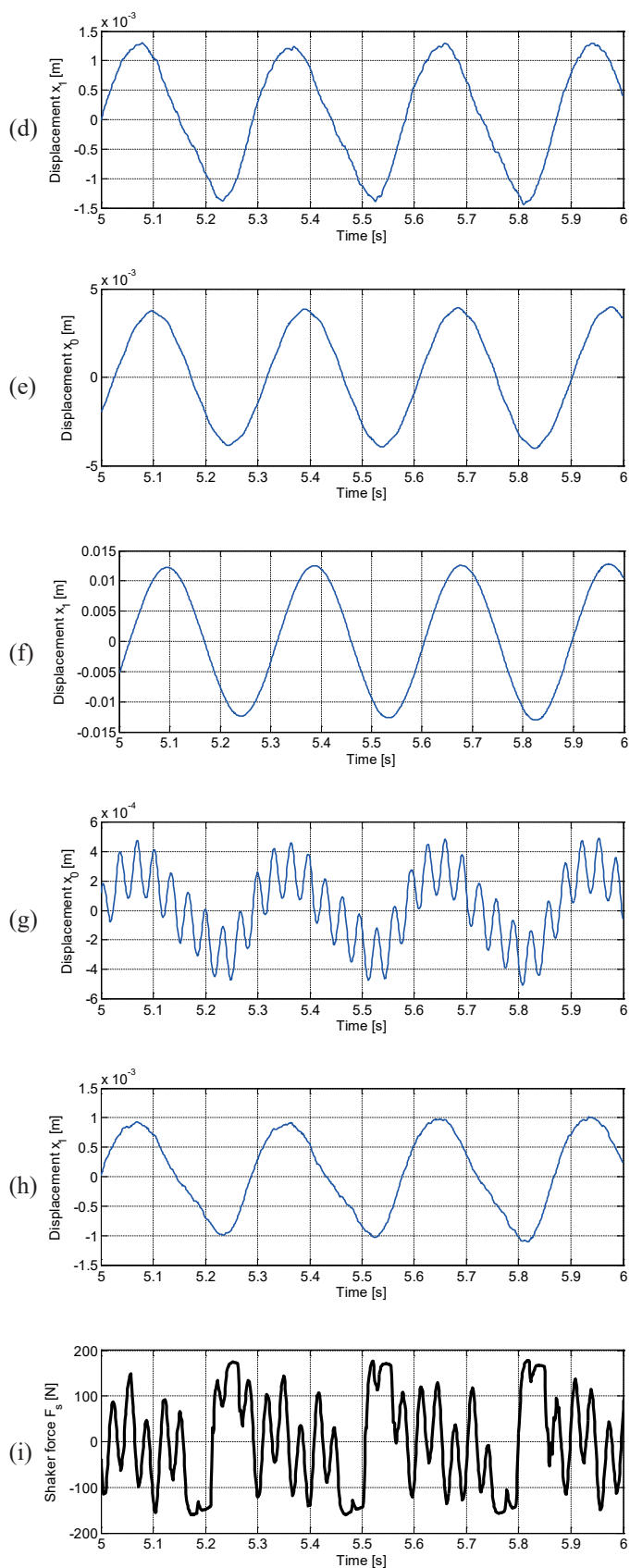Fig. 21. Tower midpoint x_0, and tower tip x_1 displacement responses to polyperiodic excitation for the system: (a)(b) 0.0 A, (c)(d) 0.1 A, (e)(f) TVA locked, (g)(h) Mod.GND 0.5, and (i) excitation signal
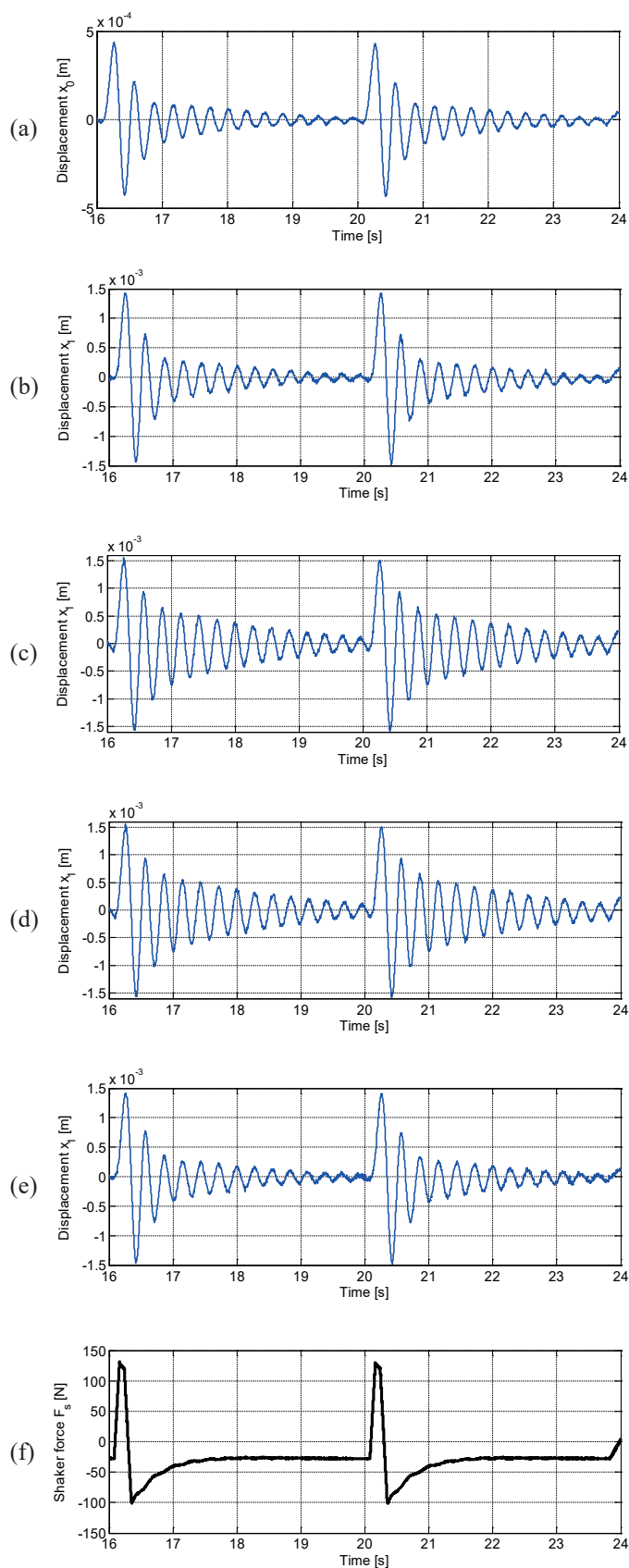
Fig. 22. Tower midpoint x_0, and tower tip x_1 displacement responses to impulse excitation for the system: (a)(b) 0.0 A, (c) 0.1 A, (d) TVA locked, (e) Mod.GND 0.5, and (f) excitation signal

Table 2. Results of impulse, polyperiodic and random excitation tests (description in text)

System / Index	Impulse Excitation				Polyperiodic Exc.		Random Excitation	
	RMS(x₁) [mm]	RMS(x₀) [mm]	(max(x₁)−min(x₁))/2 [mm]	(max(x₀)−min(x₀))/2 [mm]	A(x₁) [mm]	A(x₀) [mm]	RMS(x₁)/RMS(Fs) [10⁻²mm/N]	RMS(x₀)/RMS(Fs) [10⁻²mm/N]
0.0A	**31.6464**	**9.5588**	**1.4805**	**0.4353**	**0.8984**	**0.2908**	1.5051	0.4906
0.1A	39.5943	12.0120	1.5924	0.4672	1.3260	0.4354	1.5398	0.4921
0.2A	51.4572	15.5520	1.7323	0.5057	2.0200	0.6091	1.4783	0.4912
TVA Locked	67.8168	20.5785	1.9352	0.5822	12.6505	3.9353	1.5252	0.4871
1C INV	32.5444	9.8562	1.4848	0.4383	1.0802	0.3568	1.4520	0.4697
ADAPT 0.6C INV	34.5337	10.4387	1.5053	0.4437	1.4623	0.5130	1.4454	0.4647
GND 0.25	32.4864	9.8265	**1.4814**	0.4417	1.0628	0.3126	1.5516	0.4945
Mod.GND 0.25	32.1046	9.7439	**1.4720**	0.4389	**0.9640**	0.3050	1.5056	0.4961
Mod.GND 0.5	**31.9816**	**9.6921**	**1.4626**	**0.4359**	1.0247	0.3413	1.5122	0.4955
C3 150 INV	32.7133	9.9012	1.4841	0.4403	0.9746	**0.2995**	1.4690	0.4689
SQRT 0.15 INV	33.9485	10.2143	1.5200	0.4470	1.0488	0.3127	1.4521	0.4717
SMC 0.25	40.9402	12.4025	1.6061	0.4767	1.3773	0.4012	1.4486	0.4784
LQG INV	32.7258	9.9070	**1.4706**	0.4380	1.2879	0.4605	1.6252	0.5553

www.czasopisma.pan.pl   PAN   www.journals.pan.pl

Study of vibration control using laboratory test rig of wind turbine tower-nacelle system with MR damper based tuned vibration absorber

x_0 and x_1 impulse responses for the passive system with 0.0 A control current, and x_1 impulse responses for the system with 0.1 A, system with "locked" TVA, and for the system with Mod. GND algorithm (time patterns of x_0 are similar to the respective patterns of x_1), as well as the excitation force F_s pattern.

The above results are slightly compromised as shaker was connected to the analyzed tower-nacelle model with the help of drive train system during the entire test. After impulse excitation, shaker armature damping influenced the response profile. To cope with that problem, free vibration reduction was considered as a following test with drive train system disconnected from the vibrating structure. Figs. 23–26 present results of such an analysis for selected open loop and feedback systems.

The problem of producing adequately large force excitation signals with high frequency content along with shaker armature damping also concerned semi-random excitation tests, including Davenport or Kaimal spectrum [32, 33], which were considered to model wind speed and aerodynamic forces acting on the wind turbine. Using power spectrum estimates [33], sever-
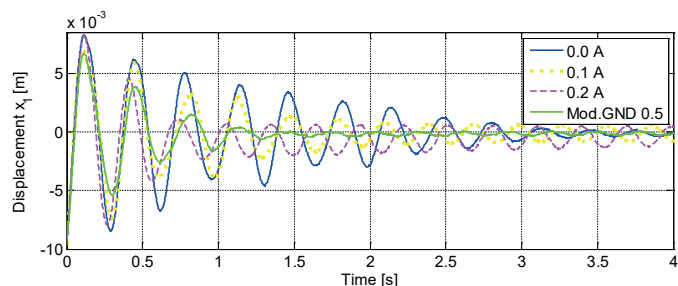

Fig. 23. Tower tip x_1 displacements time patterns – free vibration response (details in the text and in the legend)
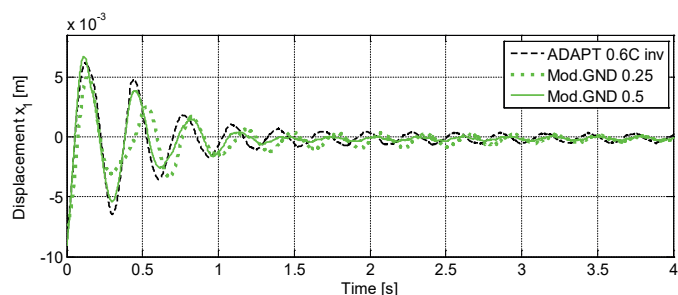

Fig. 24. Tower tip x_1 displacements time patterns – free vibration response
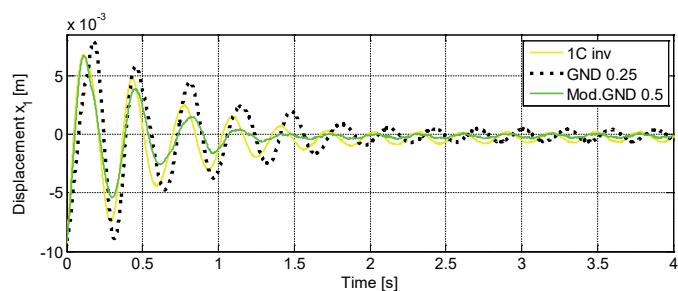

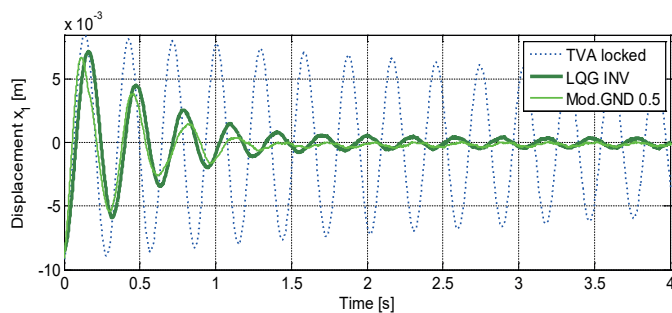Fig. 25. Tower tip x_1 displacements time patterns – free vibration response

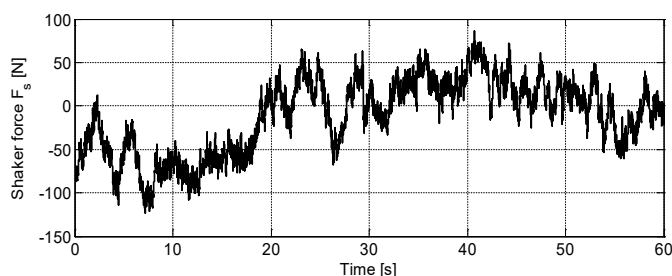Fig. 26. Tower tip x_1 displacements time patterns – free vibration response

Fig. 27. Excitation realization profile generated using Davenport spectrum

al semi-random realizations were generated as a superposition of thousands of sine waves of different frequencies, random phases and amplitudes corresponding to the power of the particular frequency in the spectrum. The exemplary excitation realization profile generated using Davenport spectrum [33] is presented in Fig. 27 (patterns containing higher force content failed to be reproduced by the shaker). Time responses to such excitation profile were gathered, yet amplitudes of MR damper relative displacement were marginally small for both F_s and P_s semi-random excitation, so the results presented in Table 2 (RMS displacements divided by RMS force F_s) concerning vibration control are questionable (typed in grey font). According to the above remark, presentation of P_s excitation results was omitted for this test.

6. Conclusion

The conducted experimental study along with analyses results presented in other publications, e.g. [24–26], all confirm the sense and advisability of the proposed implementation of MR TVA in a wind turbine nacelle assembly, based on investigation of tower-nacelle model. The potential of MR TVA in tower-nacelle structural vibration reduction at frequency of the 1st bending mode is significant. Vibration control results of the system equipped with MR TVA are improved in relation to the system that emulates standard TVA with linear (viscous) damper, and with passive solutions with constant MR damper input current.

As can be observed, *Mod.GND 0.5* algorithm delivers the most preferable responses, and its results are reasonably good over a wide variety of tests, most of all for excitation within

1st bending frequency f_1 neighbourhood range, where a slight improvement may be possible for (3.15, 3.90) Hz range only, which is demonstrated by very low MR damper input current solutions as *C3 150 INV Fr* or, obviously, 0.0 A open loop system. These solutions, however, suffer from high amplitudes below and above frequency f_1. The typical for TVA two maxima of frequency characteristics can be clearly observed not only for the open-loop system 0.0 A and some nonlinear damping control solutions, but also for linear damping *0.6C PI1 Fr* (although not for 1C), or adaptive control *ADAPT 0C INV Fr* algorithms, i.e. only for the solutions with low damping (e.g. reduced by the factor of 0.6 or zero required damping). The hardly measurable structure inherent damping resulting from, among others, interfacial friction in joints, shaker armature and drive train system damping, linear bearings friction, MR damper sealing and pre-yield friction component, all of them compromised the shape/presence of two apparent maxima of frequency characteristics for some systems. It was also observed that including hysteresis in MR damper inverse model generally improves vibration response of algorithms determining damper desired force (*C, C3, SQRT, ADAPT*), in relation to the use of inverse model without hysteresis.

More analyses are concerned regarding control solutions, among other improving MR damper force tracking algorithm by combining PID-family controller with direct force measurement and improved MR damper inverse model, using Kalman filter [31] for real-time reproduction of velocity signals (especially) [34], and conducting more valuable random excitation tests.

References

[1] I. Enevoldsen and K.J. Mork, "Effects of vibration mass damper in a wind turbine tower", *Mech. Struct. & Mach.* 24 (2), 155–187 (1996).

[2] P. Jain, *Wind Energy Engineering*, McGRAW-HILL (2011).

[3] U.A. Butt and T. Ishihara, "Seismic load evaluation of wind turbine support structures considering low structural damping and soil structure interaction", *European Wind Energy Association Annual Event*, Copenhagen (2012).

[4] M.H. Hansen, P. Fuglsang, K. Thomsen, and T. Knudsen, "Two methods for estimating aeroelastic damping of operational wind turbine modes from experiments", *European Wind Energy Association Annual Event*, Copenhagen (2012).

[5] F. Matachowski and P. Martynowicz, "Analiza dynamiki konstrukcji elektrowni wiatrowej z wykorzystaniem środowiska Comsol Multiphysics", *Modelowanie Inżynierskie* 13 (44), 209–216 (2012).

[6] C. Bak, R. Bitsche, A. Yde, T. Kim, M.H. Hansen, F. Zahle, M. Gaunaa, J. Blasques, M. Dossing, J.J. Wedel-Heinen, and T. Behrens, "Light rotor: the 10-MW reference wind turbine", *European Wind Energy Association Annual Event*, Copenhagen (2012).

[7] W. Shan and M. Shan, "Gain scheduling pitch control design for active tower damping and 3p harmonic reduction", *European Wind Energy Association Annual Event*, Copenhagen (2012).

[8] M. Jelavić, N. Perić, and I. Petrović, "Damping of wind turbine tower oscillations through rotor speed control", *International Conference on Ecologic Vehicles & Renewable Energies*, Monaco (2007).

[9] H. Namik and K. Stol, "Performance analysis of individual blade pitch control of offshore wind turbines on two floating platforms", *Mechatronics* 21, 691–703 (2011).

[10] J.P. Den Hartog, *Mechanical Vibrations*, Dover Publications, Mineola, NY 1985.

[11] S. Oh and T. Ishihara, "A study on structure parameters of an offshore wind turbine by excitation test using active mass damper", *EWEA Offshore*, Frankfurt 2013.

[12] A. Tsouroukdissian, C.E. Carcangiu, I. Pineda Amo, M. Martin, T. Fischer, B. Kuhnle, and M. Scheu, "Wind turbine tower load reduction using passive and semiactive dampers", *European Wind Energy Association Annual Event*, Brussels 2011.

[13] M.A. Rotea, M.A. Lackner, and R. Saheba, "Active structural control of offshore wind turbines", *48th AIAA Aerospace Sciences Meeting Including the New Horizons Forum and Aerospace Exposition*, Orlando (2010).

[14] W. Łatas and P. Martynowicz, "Modelowanie drgań układu maszt-gondola elektrowni wiatrowej z tłumikiem dynamicznym", *Modelowanie Inżynierskie* 13 (44), 187–198 (2012).

[15] P.H. Kirkegaard et al., "Semiactive vibration control of a wind turbine tower using an MR damper", *Struct. Dynamics EURODYN 2002*, Grundmann&Schueller, Swets&Zeitlinger, Lisse (2002).

[16] S. Kciuk and P. Martynowicz, "Special application magnetorheological valve numerical and experimental analysis", *Diffusion and Defect Data – Solid State Data. Pt. B, Solid State Phenomena* 177 (Control engineering in materials processing), 102–115 (2011).

[17] Lord Rheonetic, *MR Controllable Friction Damper RD-1097-01 Product Bulletin*, Lord Co. 2002.

[18] J. Snamina and B. Sapiński, "Energy balance in self-powered MR damper-based vibration reduction system", *Bull. Pol. Ac.: Tech.* 59 (1), 75–80 (2011).

[19] P. Martynowicz, "Development of laboratory model of wind turbine's tower-nacelle system with magnetorheological tuned vibration absorber", *Solid State Phenomena*, 208, 40–51 (2014).

[20] J. Snamina, P. Martynowicz, and W. Łatas, "Dynamic similarity of wind turbine's tower-nacelle system and its scaled model", *Solid State Phenomena*, 208, 29–39 (2014).

[21] P. Martynowicz and Z. Szydło, "Wind turbine's tower-nacelle model with magnetorheological tuned vibration absorber: the laboratory test rig", *Proceedings of the 14th International Carpathian Control Conference*, 238–242 (2013).

[22] TMS, *60 Lbf Modal Shaker*, The Modal Shop Inc. 2010.

[23] M. Rosol and P. Martynowicz, "Identification of Wind Turbine Model with MR Damper Based Tuned Vibration Absorber", Journal of Dynamic Systems, Measurement and Control (in review).

[24] P. Martynowicz, "Wind turbine's tower-nacelle model with magnetorheological tuned vibration absorber–-numerical and experimental analysis", *6WCSCM:Sixth World Conference on Structural Control and Monitoring: proceedings of the 6th edition of the World conference of the International Association for Structural Control and Monitoirng (IACSM): Barcelona, Spain*, ISBN: 978-84-942844-5-8 (2014).

[25] J. Snamina and P. Martynowicz, "Prediction of characteristics of wind turbine's tower-nacelle system from investigation of its

www.czasopisma.pan.pl PAN www.journals.pan.pl

Study of vibration control using laboratory test rig of wind turbine tower-nacelle system with MR damper based tuned vibration absorber

scaled model", *6WCSCM:Sixth World Conference on Structural Control and Monitoring: proceedings of the 6th edition of the World conference of the International Association for Structural Control and Monitoirng (IACSM): Barcelona, Spain*, ISBN: 978-84-942844-5-8 (2014).

[26] P. Martynowicz, "Vibration control of wind turbine tower-nacelle model with magnetorheological tuned vibration absorber locked", *Journal of Vibration and Control*, DOI: 10.1177/1077546315591445 (2015).

[27] H. Laalej, Z.Q. Lang, B. Sapinski, and P. Martynowicz, "MR damper based implementation of nonlinear damping for a pitch plane suspension system", *Smart Mater. Struct*. 21, DOI: 10.1088/0964–1726/21/4/045006 (2012).

[28] C. Ho, Z. Q. Lang, B. Sapinski, and S.A. Bilings, "Vibration isolation using nonlinear damping implemented by a feedback-controlled MR damper", *Smart Mater. Struct.* 22, DOI: 10.1088/0964-1726/22/10/105010 (2013).

[29] T. Orlowska-Kowalska and G. Tarchala, "Unified approach to the sliding-mode control and state estimation – application to the induction motor drive", *Bull. Pol. Ac.: Tech.* 61 (4), 837–846 (2014).

[30] V.A. Neelakantan and G.N. Washington, "Vibration control of structural systems using MR dampers and a 'modified' sliding mode control technique", *J. Intell. Mater. Syst. Struct.* 19 (2), 211–224 (2008).

[31] M. Rosół and P. Martynowicz, "Implementation of LQG controller for wind turbine tower-nacelle model with MR tuned vibration absorber", *Journal of the Theoretical and Applied Mechanics* (accepted for publication).

[32] T. Ackermann, *Wind Power in Power Systems*, ISBN: 978-0-470-01267-3, J. Wiley, 2005.

[33] D. Hiriart, J.L. Ochoa, and B. Garcia, "Wind power spectrum measured at the San Pedro Martir Sierra", *Revista Mexicana de Astronomia y Astrofisica* 37, 213–220 (2001).

[34] P. Martynowicz, "Control of an MR Tuned Vibration Absorber for Wind Turbine Application Utilising the Refined Force Tracking Algorithm", *Low Frequency Noise*, Vibration, and Active Control (in review).